Appl. Phys. B 71, 85–94 (2000) / Digital Object Identifier (DOI) 10.1007/s003400000214

Applied Physics B
Lasers
and Optics

Collisional processes near the CH $B\,^2\Sigma^-$ $v' = 0, 1$ predissociation limit in laser-induced fluorescence flame diagnostics

J. Luque, R.J.H. Klein-Douwel, J.B. Jeffries, D.R. Crosley

Molecular Physics Laboratory, SRI International, 333 Ravenswood Avenue, Menlo Park, CA, 94025, USA

Received: 24 September 1999/Published online: 7 June 2000 –

Abstract. Excitation and dispersed laser-induced fluorescence spectra of CH $B\,^2\Sigma^- v' = 0, 1$ in methane flames are analyzed using rotational relaxation models to investigate their applicability for flame diagnostics. The existence of non-predissociative and highly predissociative rotational levels in the same vibrational state provides a unique scenario to test the effects of rotational relaxation in laser-induced fluorescence measurements. Using a statistical power gap law for rotational relaxation modeling, we find that the levels with collision-free lifetimes as short as 100 ps have apparent fluorescence yields larger than expected because of the extent of rotational relaxation at atmospheric pressure. Also, vibrational ($v' = 1$ to $v' = 0$) and electronic energy transfer (B $^2\Sigma^- v' = 1$ to A $^2\Delta$) are competitive, and together are half the value for the total collisional removal rate from CH $B\,^2\Sigma^- v' = 0$. The measured electronic energy transfer branching ratio into A ($v' = 0 - 3$) depends on the initial rotational level pumped, and energy gap considerations can be used to explain these propensities. The combination of measurements and model calculations finds the excitation of the CH $B\,^2\Sigma^-$ $v' = 1$, $N' = 8$ level a good candidate for laser-induced fluorescence quantitative measurements in flames at atmospheric pressure.

PACS: 42.62.Fi; 34.50.Ez; 33.80.Gj; 33.20.Lg

1 CH laser-induced fluorescence in combustion diagnostics

In combustion diagnostics, the CH radical is studied because of its role in the formation of prompt NO and as a means to locate either flame fronts or hydrocarbon reaction areas. This radical was the first combustion intermediate to be studied by laser-induced fluorescence (LIF) [1] and the second by planar laser-induced fluorescence (PLIF or 2-D LIF) [2]. Excitation/detection schemes in these experiments generally determine the quality of the final data. Many different factors are relevant, and the choice is often a compromise among all the variables. Signal level is always important, but quite often the fluorescence appears along with photochemical interference, Rayleigh, Mie, and Raman scatterings. In other cases, the sample self-absorption might preclude the use of the strongest bands. The fluorescence quantum yield usually varies with quenching, which depends on temperature, composition, and pressure. Two methods to reduce the collisional effects are saturation and competitive predissociation. Fluorescence saturation has the inconvenience of loss of spatial resolution because of the so-called "wing" effects. Competitive predissociation is only available for selected states of a few molecules, OH A $v' = 3$ being the most common example [3, 4].

Different schemes have been used for CH planar laser-induced fluorescence measurements, taking advantage of the availability of three different electronic transitions, A−X, B−X, and C−X, in the near ultraviolet and visible. In the A−X system, diagonal approaches pumping the (0,0) band are common [2, 5–8], but they might suffer from Rayleigh and Mie scattering problems because excitation and detection are in the same spectral region. In some cases, the scattering problem has been reduced by using interference filters; collecting fluorescence from the Q branch after pumping either the R or P branch [5, 8], but the signal is decreased by 80% and fluorescence polarization effects might be large [9]. Off-diagonal schemes have been developed to overcome these problems. Paul and Dec [10] pumped A−X(1,0) and detected the (1,1) and (0,0) bands. The A−X(1,0) band has an oscillator strength about 1000 times smaller than that of diagonal bands [11], requiring high laser powers to reach workable signal levels. Namazian et al. [12] excited the (0,0) band and observed the (0,1) band; this approach faces the possible problem that only 2% of the fluorescence is emitted at this band. Moreover, Raman scattering signals from species like CH_4 overlap with this low intensity fluorescence signal. Finally, Bergeman et al. [13] excited the (0,1) band and detected the (0,0). In this case, the (0,1) oscillator strength is about 40 times smaller than that of (0,0) band. Unfortunately, this scheme suffers from a high temperature dependence of the signal because the population in CH X $v'' = 1$ changes abruptly with this factor. Also, the population in $v'' = 1$ is only

5% to 15% of that in $v'' = 0$ in the temperature range of 1300–2200 K.

The C−X system possibilities for PLIF have been investigated by Hirano and coworkers [14, 15]. The C state is highly diagonal [16], as in the A state case [17]. It predissociates in all rotational and vibrational levels, and the predissociation rate is fast enough to compete with quenching rates typical of combustion environments at atmospheric pressure [18, 19]. Exciting the (0,0) band, the fluorescence was collected in two different ways; from the (0,1) band, and from the A−X (0,0) transition, which is produced by electronic energy transfer C → A [20]. Both methods minimized scattering and background optical emission effects. However, the former scheme collects only 0.5% of the fluorescence [16], and the latter might depend on temperature, pressure, and composition because very little is known about the C → A collisional transfer mechanism. Exciting the C−X (1,0) band and collecting the (1,1) and (0,0) fluorescence, has the advantage over the $(0, 0) \rightarrow (0, 1)$ scheme, because the predissociation is three times faster in $v' = 1$ than in $v' = 0$ [19], and the amount of total signal will be larger with the (0,0) and (1,1) fluorescence collection.

The B state is slightly different from the A and C states. First, it is very shallow, with only two bound vibrational levels. Second, it predissociates through a potential barrier, so that the predissociation rates vary with rotational level and can be very fast. The B−X system has been used by Carter et al. [21] and Klein-Douwel et al. [22] in PLIF experiments. They excited the B−X (0,0) band and collected light in the B−X (0,1) and A−X spectral region. The percentage of fluorescence emitted by the B−X (0,1) band is about 3.5% [17]. The electronic energy transfer B → A has been measured to be 20% of the total collisional removal from B [23], and thus most of the fluorescence collected at atmospheric pressure will come from the A−X emission at 431 nm. This approach has been shown to be no more temperature, composition, and pressure dependent than the direct monitoring of fluorescence from CH B [24].

The vibrational level $v' = 1$ in the B state shows diagnostic advantages over $v' = 0$. The combination of the electronic transition moment variation and large anharmonicity of the state results in an emission coefficient for the (1,0) band that is about the same as that of the (1,1) band. The predissociation onset is at $N' = 7$ and the rotational levels most commonly excited for combustion diagnostics, which are $N' = 7 - 10$ because of their fractional populations are nearly temperature independent, have collision-free lifetimes of 5, 0.3, 0.06, and 0.015 ns respectively (see Table 1). These levels are very attractive for laser-induced predissociative fluorescence applications. In $B\,^2\Sigma^- v' = 0$, the predissociation appears at $N' > 14$, requiring too high an N'' for practical combustion diagnostics applications.

In a previous study, we determined the influence of rotational relaxation when non-predissociative levels near the predissociation limit in $CH\,B\,^2\Sigma^- v' = 0$ are excited [25]. Using spectral simulation and a model of rotational relaxation, we found that deviations in temperature determinations of nearly 10% can occur, because a non-negligible fraction of the excited molecules are transferred by collisions to levels beyond the predissociation limit. This effect becomes more important as the level pumped is closer to the predissociation onset. The present work deals with levels excited beyond the predissociation limit. First, we reanalyze data from laser-induced fluorescence excitation scans used for the determination of predissociation rates. We show that the application of the rotational relaxation model brings experimental and calculated predissociation rates for $CH\,B\,^2\Sigma^- v' = 0, 1$ into even better agreement. Second, we investigate the feasibility of performing laser-induced fluorescence (LIF) in the predissociative levels of $CH\,B\,^2\Sigma^- v' = 1$ for combustion diagnostics at atmospheric pressure. We evaluate the effects of rotational energy transfer (RET), vibrational energy transfer (VET), and electronic energy transfer (EET) upon the fluorescence yield of $CH\,B\,^2\Sigma^- v' = 1$ for this application.

2 Experimental

All the laser-induced fluorescence data were recorded in hydrocarbon flames, but with two very different collisional conditions. The first set of data was collected for previous experiments, aspects of which have been published [11, 17, 25, 26]; a CH_4/O_2 flame with an equivalence ratio of 1.08 at 8 Torr in a Mckenna burner is the target system. The CH was excited at the position in the flame at peak of its number density distribution. A dye laser pumped with a Nd:YAG (temporal width 6 ns, spectral bandwidth $\approx 0.2\,\mathrm{cm}^{-1}$, vertically polarized) is used to excite CH in the B−X (0,0) and (1,1) bands. The fluorescence was detected with monochromators and photomultipliers, and the signal was either time integrated or over some gate width or time resolved with a transient digitizer. The spectral resolution varied from 0.5 nm for the B−X (0,0) and 0.9 nm for the B−X (1,1), to 30 nm to collect the entire band for the excitation LIF scans. Some quenching data are taken from a $CH_4/O_2/N_2$ ($O_2/(N_2 + O_2) = 0.3$) flame at 25 Torr pressure in the same Mckenna burner.

The second set of data is from a partially premixed CH_4/air Bunsen flame, burning at atmospheric pressure at an equivalence ratio of 1.36 in the premixed inner cone. The CH B−X (1,0) transition at 365 nm is excited with a dye laser Lambda Physik FL-2002 (temporal width ≈ 14 ns, spectral bandwidth $\approx 0.2\,\mathrm{cm}^{-1}$, vertically polarized), pumped by a XeCl excimer laser Lambda Physik EMG 103 MSC. The path of the laser beam through the Bunsen flame is imaged, after passing a depolarization filter, onto a spectrograph SPEX 270M ($f/4$, 500 nm blaze angle) with a gated intensified CCD camera (Princeton Instruments, ICCD-576G/RBT, 14 bits dynamic range, 384×576 pixels, pixel size 23 μm). This signal is spectrally dispersed along the horizontal direction of the array. The spectral resolution is 0.25 nm FWHM (about four camera pixels), determined from the Hg line at 404.6 nm, and the instrumental lineshape can be represented by a linear combination of Gaussian (80%) and Lorentzian profiles (20%). The vertical direction in the collected images corresponds to the horizontal position along the path of the laser beam, which enables spatial resolution of the fluorescence images. One CCD pixel corresponds to 20 μm in the flame, but the imaging of a test card indicates the spatial resolution of our optical collection system is approximately 25 pixels or 500 μm.

Table 1. Collision-free lifetimes from experiments and calculations for CH B $v' = 0, 1$ (in ns)

CH B $v'=0$	Experiment			Theory		
N'	Kumar et al. [35]	Luque and Crosley [26]	Brzozowski [19]	Brooks and Smith [43]	Elander et al. [34]	Szalay and Nemes [36]
14		375 ± 40	371 ± 10	400		
15		160 ± 40	130 ± 10	100 ± 20	128	23.7
16		10 ± 5			5.88	1.53
17		1.3 ± 1			0.495	0.16
18					0.064	0.021
19	0.010 ± 0.002				0.0107	0.004
20	0.003 ± 0.001					0.001
21	~ 0.0012					
CH B $v'=1$	Experiment			Theory		
N'	Kumar et al. [35]	Luque and Crosley [26]	Herzberg and Jones [32, 34]	Elander et al. [34]	Szalay and Nemes [36]	
6		398 ± 80			1.45	
7		8 ± 4		4.57	0.267	
8		0.9 ± 0.6	0.270	0.368	0.061	
9			0.053	0.066	0.016	
10	0.014 ± 0.02		0.013	0.0162	0.0045	
11	0.008 ± 0.003		0.0067	0.0047	0.0013	
12	~ 0.0017		0.0021	0.0015	0.0005	
13	~ 0.0009			0.00055	0.0002	

The useful dispersed fluorescence scans span from 380 to 470 nm, where the B−X (0,0), (1,1), (0,1), and (1,2) as well as the A−X (0,0), (1,1), and (2,2) bands are readily detected. Composites of three spectra with some overlapping wavelength regions are recorded to cover this range. Appropriate background images of the dark current of the CCD camera and of the natural emission of the flame are recorded and subtracted from the dispersed fluorescence images. The gate of the image intensifier is set to 200 ns, wide enough to include any excimer laser jitter and minimize the flame optical emission. The wavelength axes of the images are calibrated for each grating setting separately, using known wavelengths of either Raman signals from O_2, N_2, CH_4, or optical flame emission. The system spectral response in this region is obtained from the branching ratio B−X(1,1)/B−X(1,2), which is known to be 0.165 ± 0.02 [17] but is found experimentally before correction to be 0.20 ± 0.01. Therefore, the spectral response varies 20% over the range from 405 nm to 455 nm, and we interpolate linearly to correct the intensities over this region.

Partially polarized fluorescence is expected from the B−X $(1, v'')$ bands after B−X (1,0) laser excitation [27–29]. Depending on the excitation/detection geometric scheme, laser light polarization, and fluorescence degree of polarization, the effects of polarized fluorescence in dispersed fluorescence scans can be large [9]. In the present experiment, the laser light is vertically polarized and the fluorescence detected is $I_v = (1/2)I_\perp + (1/2)I_\parallel$, which is close to the ideal isotropic distribution $I_{iso} = (2/3)I_\perp + (1/3)I_\parallel$. Preliminary measurements estimate the degree of polarization for the $Q_1(8)$ line excitation to be $P = 0.2 - 0.25$ compared to a maximum value of 0.5 [9]. Calculations for Q lines laser excitation show that intensity deviations by partial polarization of the fluorescence are expected to be 10% or less between R, P, and Q branches. Thus, corrections to the dispersed fluorescence scans are not necessary to extract valid information.

3 Laser-induced fluorescence model with rotational relaxation in the excited state

After exciting from the ground state k to the excited state level i in a manifold of rotational levels each denoted by j, the laser-induced fluorescence signal is:

$$S_{\mathrm{LIF}}(\mathrm{k}, t) = \sum_{\mathrm{j}} n_{\mathrm{j}}(t) A_{\mathrm{jk}}\,, \tag{1}$$

where levels other than i are populated by RET. The individual rotational populations n_j are obtained by the solution of the set of coupled linear differential equations, assuming the optical excitation to be in the linear regime:

$$\frac{\mathrm{d}n_{\mathrm{i}}}{\mathrm{d}t} = -(A_{\mathrm{i}} + Q_{\mathrm{i}} + P_{\mathrm{i}})n_{\mathrm{i}} + B_{\mathrm{ki}} I(t) n_{\mathrm{k}} + \sum_{\mathrm{i}\neq\mathrm{j}} (R_{\mathrm{ji}} n_{\mathrm{j}})\,. \tag{2}$$

Here A_i is the emission coefficient, Q_i is the quenching rate, P_i is the predissociation rate, all in s^{-1} units, n_k is the population in the ground state, $I(t)$ the laser spectral irradiance, assumed to be a Gaussian with the known laser temporal width, and B_{ki} is the absorption coefficient between the levels k and i. The R_{ij} correspond to the state-specific rotational relaxation rates, which are modeled by a statistical power-gap law (SPG). This model was introduced by us for CH RET in a flame in a previous work [25] and shown there to be slightly better than an exponential gap law [30, 31]. With this model,

$$R(N_{\mathrm{i}} \to N_{\mathrm{j}}) = (2N_{\mathrm{j}} + 1)\mathrm{e}^{\left(\frac{(E_{\mathrm{i}} - E_{>})}{kT}\right)} a \left(\frac{|E_{\mathrm{j}} - E_{\mathrm{i}}|}{B_{\mathrm{v}}}\right)^{-\alpha}\,, \tag{3}$$

where the first two terms ensure microscopic reversibility. $E_>$ is the larger of E_j and E_i, T is the temperature, B_v is the rotational constant of the excited electronic/vibrational state, a and α are adjustable parameters, a depends on pressure and temperature, but α does not.

Because of the barrier tunneling predissociation mechanism, first suggested by Herzberg [32], the predissociation rates P_i vary rapidly with rotational number, resulting in collision-free lifetimes that change almost one order of magnitude from level to level. Table 1 compiles the available measurements and calculations. Emission coefficients, line positions and simulation routines are from the LIFBASE program [33].

4 CH B $^2\Sigma^-$ $v' = 0, 1$ predissociation rates reanalysis

The predissociation rates were studied in the 8-Torr methane/oxygen flame exciting the CH B−X (0,0) and (1,1) transitions in the flame front at 1950 K, at the peak of the 6-mm FWHM CH distribution, using 1–2 mm spatial resolution. Rotational relaxation in this flame has been modeled and the SPG parameters that represented the rotational relaxation were $\alpha = 1.2$ and $a = 4 \times 10^7\ s^{-1}$, while the quenching rate was measured to be $8 \times 10^6\ s^{-1}$ [25]. LIF excitation scans provided the data to extract the predissociation rates (see Fig. 1 in [26]). To avoid large influence from RET, an integration gate of 40 ns, relatively short compared to the effective lifetime of ≈ 100 ns, was used to integrate the fluorescence. Dispersed fluorescence scans were also taken with this integration gate. For all the levels initially excited by the laser, nearly the same percentage of the total fluorescence was collected from levels populated by RET, leading to the preliminary conclusion that rotational effects were similar no matter the specific pumped level. However, this approximation failed to account for the fact that, when pumping a non-predissociative level, some fluorescence was missing because of the RET beyond the predissociation limit. Conversely, when pumping a predissociative level, there was some additional fluorescence from molecules transferred to lower non-predissociative levels by RET, and those levels had a much higher effective quantum yield. These opposite effects do not cancel out, and in the analysis of the excitation scans to obtain predissociation rates, the resultant collision-free lifetimes are longer than expected.

Table 2. Experimental and calculated excitation LIF intensities for the CH B $v' = 0, 1$ P(N') lines at 1950 K and 8 Torr pressure

CH B $v' = 0$ N'	Experiment	LIF with rotational relaxation model	
		With Elander et al. lifetimes [34]	With Luque and Crosley lifetimes [26]
13	1.00	1.000	1.000
14	0.75	0.715	0.721
15	0.50	0.448	0.462
16	0.11	0.119	0.159
17	0.01	0.009	0.022
CH B $v' = 1$ N'			
5	1.00	1.000	1.000
6	0.94	0.824	0.839
7	0.19	0.230	0.340
8	0.02	0.019	0.045

To illustrate this point we modeled the excitation scans including rotational relaxation using two different sets of lifetimes. First, we used those that had been derived assuming negligible effects due to RET [26], which overpredicts the signal intensity for the highly predissociative levels $v' = 0$, $N = 16$, 17 and $v' = 1$, $N' = 7, 8$ (Table 2). Second, predissociative lifetimes from Elander's calculations [34] were used, and the modeled intensities agree within 20% of the experimental values. From the simulation results, we conclude that rotational relaxation effects were not totally removed from the analysis in our prior work, and that Elander's calculated predissociation rates are very close to the actual ones. The latter conclusion is reinforced by the experiments of Herzberg [32], Elander [34], and Kumar [35], which show differences of 40% or less for $v' = 0$, $N' = 19$ and $v' = 1$, $N' = 8 - 12$. There is another set of theoretical calculations by Szalay and Nemes [36], but these appear to predict the pre-

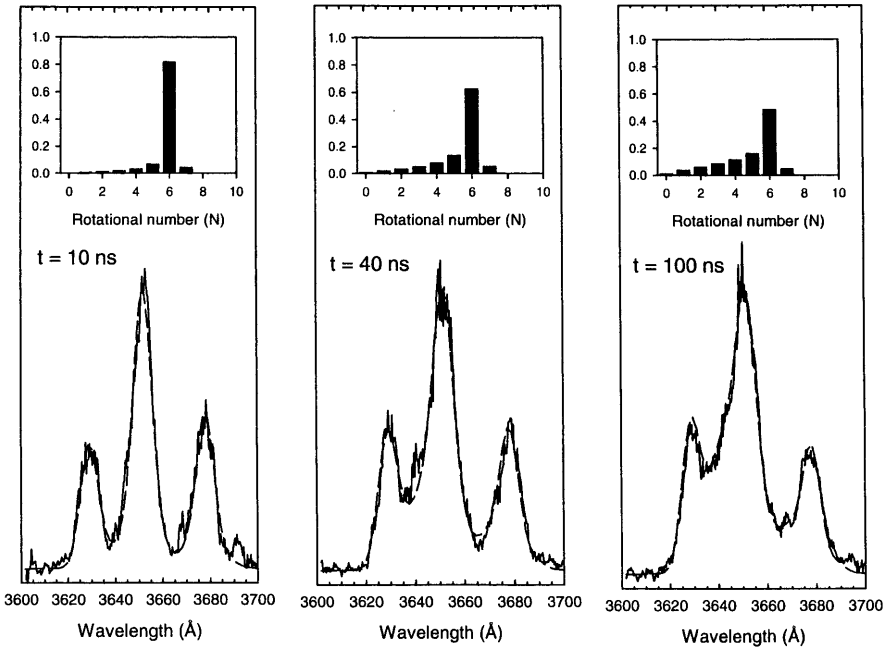

Fig. 1. CH B−X (1,0) after pumping B−X(1,1) $Q_1(6)$ in the methane/oxygen flame at 8 Torr, resolved with 0.9 nm resolution and temporal gates of 10, 40, and 100 ns from the onset of the signal (*left* to *right panels*). Experiment is *solid line*, model is *dashed line*. The histograms show the evolution of the time-integrated population

dissociation lifetimes three times shorter than all other experimental data and calculations. Figure 1 contains the time evolution of the fluorescence signal after pumping $Q_1(6)$ B−X (1,1) compared to the spectra generated by spectrum simulation and the SPG rotational relaxation model. Although the spectral resolution is not high, the model is able to reproduce the experimental spectra well.

5 CH B $v' = 1$ predissociative LIF in atmospheric-pressure flames

The CH profile in the atmospheric pressure flame is determined to be < 0.5 mm wide from spatially resolved fluorescence scans, and Rayleigh measurements together with kinetic model calculations [37] suggest that most of the CH is in a 1700–1900 K temperature region. This temperature is comparable to the value measured in the low-pressure experiment, but the composition is different because the atmospheric-pressure flame has a large amount of nitrogen in the gas feedstock.

5.1 Rotational energy transfer

Once the best available set of predissociation rates has been established, we can extend the study to atmospheric pressure using a few assumptions. Quenching in methane/O_2/N_2 ($O_2/(N_2 + O_2) = 0.3$) flames has been measured only in low-pressure conditions [38], and the rates across the flame front range between 0.44–0.55 μs^{-1} Torr^{-1} for B $^2\Sigma^-$ $v' = 0$, and 0.32–0.4 μs^{-1} Torr^{-1} for A $^2\Delta$ $v' = 0$ with a temperature gradient of 1200–1850 K. In a first approximation, the quenching for both states increases proportionally to $0.5T_1/T_2$ where $(T_1 > T_2)$. Rotational relaxation and vibrational energy transfer in CH B $v' = 0$ have been estimated in a methane/air flame [23]. The steady-state ratio RET/Q is similar to that found in methane/oxygen flames at lower pressures [25, 26], and we will use the same RET model as in the low-pressure section of the present work, scaling the parameter $a(T)$ to keep the same RET/Q ratio at any flame conditions, as has been observed for A $v' = 0$ [39]. We also use the same energy transfer parameter values for both $v' = 0$ and $v' = 1$ of B $^2\Sigma^-$.

Figures 2 and 3 display the results of the simulation compared with the dispersed fluorescence scans. Agreement is quite good for all rotational levels, and simple low-pressure data extrapolation seems sufficient for a description of the LIF in an atmospheric-pressure flame. In our first attempt to characterize RET in low-pressure flames we found the SPG model satisfactory for levels between B $v' = 0$, $N' = 8$ to $N' = 16$. However, we had no data for lower rotational levels, so we were cautious about applying the model to all rotational levels without modifying the $a(T)$ and α parameters significantly. This problem has been seen routinely in room-temperature RET experiments in diatomic molecules [31, 40]. The present results for CH B $v' = 1$, $N' = 1 - 9$ support that rotationally independent parameters and a simple model can give a fair representation of RET in B $^2\Sigma^-$. It should be noted that the SPG model gives no information about the $F_1 \leftrightarrow F_2$ transfer. However, experiments show that most of the population remains in the initially pumped spin-orbit manifold.

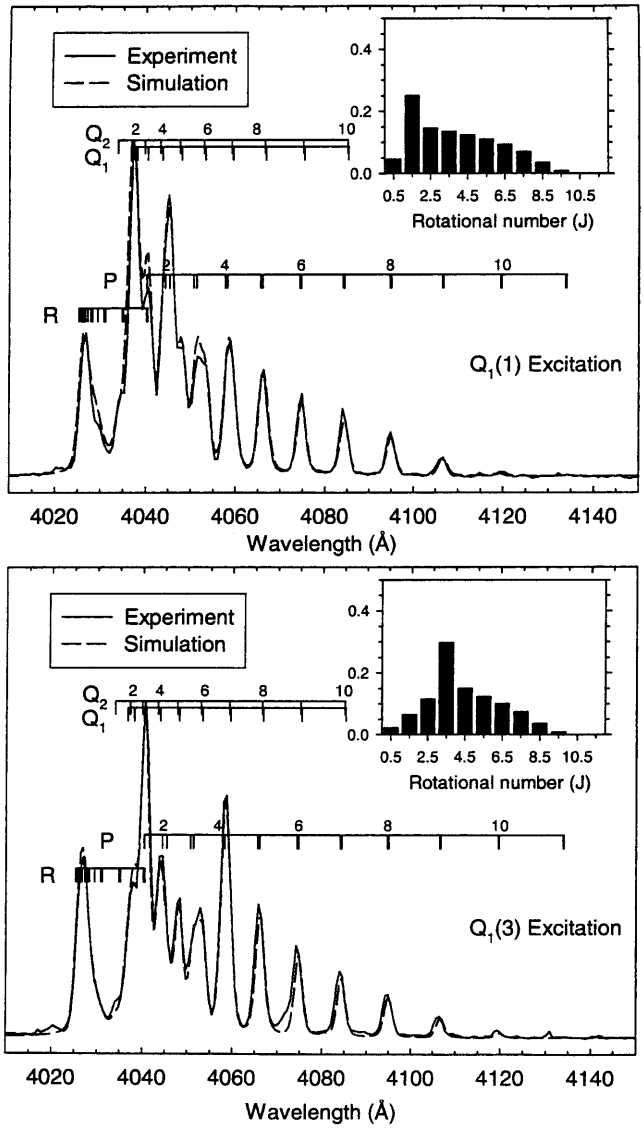

Fig. 2. Dispersed fluorescence spectra of CH B−X (1,1) after pumping $Q_1(1)$, *upper panel*, and $Q_1(3)$, *lower panel*, in the methane/air flame at atmospheric pressure resolved with 0.25 nm resolution and total time-integrated fluorescence. Experiment (*solid line*), rotational relaxation model (*dashed line*). The histograms show the rotational model time-integrated population distribution

Pumping $Q_1(1)$, we can separate some of the emission coming from F_1 and F_2 levels because the $Q_1(1)$ and $Q_2(1)$ lines are ≈ 0.3 nm apart. To reproduce the experimental spectra we have to place at least 95% of the population from the simulation model in the initially pumped spin-orbit manifold; we assume the other spin-orbit manifold roughly thermalized at 1900 K. Analogous propensity for spin-orbit conservation in a flame environment has been seen in the OH A $^2\Sigma^+$ $v' = 2$ state [28, 41].

Comparing the dispersed fluorescence spectra for non-predissociative levels (Fig. 2) and predissociative ones (Fig. 3), we observe that RET is important in both cases. For predissociative levels such as B $v' = 1$, $N' = 8$, with a collision-free lifetime ≈ 0.35 ns, there is additional fluorescence because part of the transfer populates levels below the predissociation onset. Those levels have a fluorescence

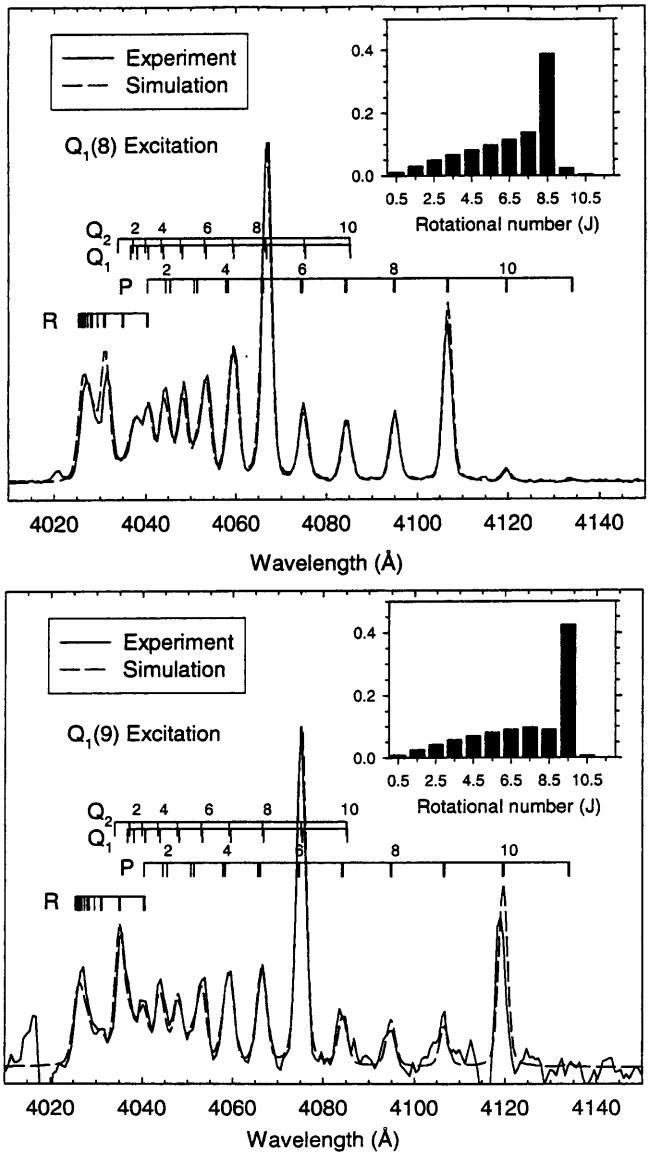

Fig. 3. Dispersed fluorescence spectra of CH B−X (1,1) after pumping $Q_1(8)$, *upper panel*, and $Q_1(9)$, *lower panel*, in the methane/air flame at atmospheric pressure resolved with 0.25 nm resolution and total time-integrated fluorescence. Experiment (*solid line*), rotational relaxation model (*dashed line*). The histograms show the rotational model time integrated population distribution

lifetime of ≈ 2–3 ns in atmospheric-pressure flame conditions and thus a larger fluorescence quantum yield than the predissociating levels. The competition between collisions and predissociation can be understood from the fact that total relaxation rate from $N' = 8$, $\Sigma_j R_{8j} \approx 10Q$, and in atmospheric flame conditions the collisional removal is 60% of the total removal rate. For $N' = 9$ and 10 the predissocation lifetime are 0.06 ns and 0.015 ns, respectively, but collisions still account for 20% and 6% of the removal rate from these rotational levels. Avoiding competition with energy transfer collisions at atmospheric pressure for flame diagnostics forces the use of highly predissociated rotational levels with very low fluorescence yields. In the present experiment, at atmospheric pressure and typical flame CH concentrations, B $v' = 1$, $N' = 8$ is readily detected, $N' = 9$ signal level is

Table 3. Methane/air flame calculated rotational fluorescence yields for CH B $v' = 1$ at atmospheric pressure and two different temperatures and energy transfer models. The temperatures are 1200 K and 1900 K. The corresponding model parameters are $a = 2.5 \times 10^6\ s^{-1}\,Torr^{-1}$ and $Q = 3.8 \times 10^8\ s^{-1}$ at 1900 K, and $a = 2.1 \times 10^8\ s^{-1}\,Torr^{-1}$ and $Q = 3.04 \times 10^8\ s^{-1}$ at 1200 K. CH B ($v' = 1$) lifetime = 420 ns [19, 44]. Fluorescence yields are multiplied by 10^3

B $v' = 1$ (N')	Fluorescence quantum yields			
	No RET		RET	
	$T = 1200$ K	$T = 1900$ K	$T = 1200$ K	$T = 1900$ K
0	7.88	6.30	3.85	2.64
1	7.88	6.30	3.82	2.61
2	7.88	6.30	3.75	2.55
3	7.88	6.30	3.66	2.48
4	7.88	6.30	3.51	2.37
5	7.88	6.30	3.31	2.23
6	7.88	6.30	3.02	2.04
7	4.57	3.99	2.46	1.69
8	0.794	0.775	1.25	0.92
9	0.155	0.154	0.34	0.29
10	0.038	0.038	0.077	0.071

low and unacceptable for most imaging applications, whereas $N' = 10$ is barely detectable.

From a diagnostics point of view, it is important to assess the fluorescence quantum yield variation due to changes in collisional rates, which are usually a function of temperature and composition. We model two different atmospheric-pressure flame conditions (Table 3, Fig. 4): a hot region, at 1900 K with quenching 0.5 $\mu s^{-1}\,Torr^{-1}$ and a cold region, at 1200 K where quenching is 0.4 $\mu s^{-1}\,Torr^{-1}$. The rotational model parameter $a(T)$ is adjusted to keep the ratio RET/Q constant with temperature. In the absence of rotational relaxation, the fluorescence yield decreases 20% from the cold to

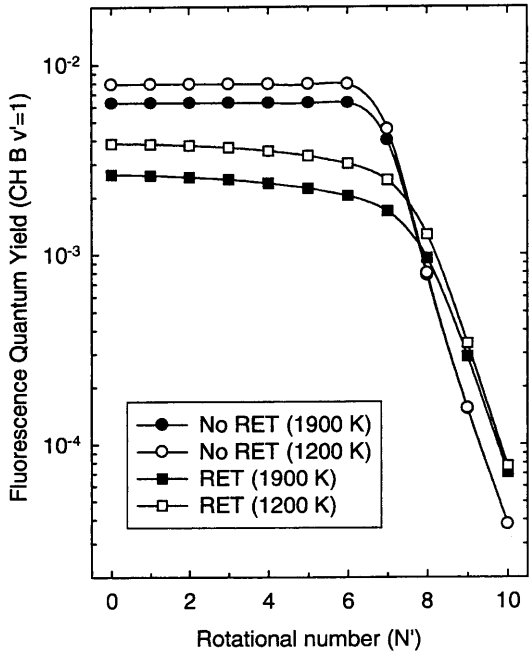

Fig. 4. CH B $v' = 1$ fluorescence quantum yields calculated at different flame temperatures with and without the rotational relaxation energy transfer model. *Circle* and *square symbols* are used to distinguish results with and without rotational relaxation

Table 4. Experimental energy transfer ratios for VET/Q and EET/Q after pumping $v' = 1$, N'. All levels excited in $Q_1(N')$ branch. The last four columns give the experimental vibrational branching ratio for the EET into the $A\,^2\Delta$ state

B $v' = 1$ (N')	$E(N')$ (cm^{-1})	$E(N')$ Averaged by RET (cm^{-1})	VET/Q B(1) → B(0)	EET/Q B(1) → A	A(0)/EET	A(1)/EET	A(2)/EET	A(3)/EET
1 $Q_2(1)+Q_{21}(1)$	23	230	0.23	0.26	0.19	0.52	0.26	≤ 0.03
1 $Q_1(1)$	23	230	0.24	0.25	0.22	0.47	0.28	≤ 0.03
3	138	266	0.26	0.25	0.18	0.51	0.28	≤ 0.03
6	480	388	0.24	0.24	0.13	0.51	0.33	≤ 0.03
7	638	468	0.24	0.22	0.16	0.48	0.33	≤ 0.03
8	817	560	0.24	0.23	0.13	0.46	0.38	≤ 0.05
9	1016	681	0.26	0.25	–	–	–	–
Average			0.24 ± 0.03	0.24 ± 0.04	0.17	0.49	0.31	≤ 0.03

the hot region for non-predissociative levels, whereas it will remain basically unchanged for highly predissociative levels. Rotational relaxation complicates this simple argument. In real flame conditions, even when one pumps a level far from the predissociation onset in B $v' = 1$, the RET promotes a large amount of population ($\approx 50\%$) beyond the predissociation limit, thereby lowering the effective fluorescence yield. When exciting highly predissociative levels, the behavior observed is the opposite, and the quantum yield is larger than expected if the analysis ignored RET. We find at flame temperatures that for $N' = 8$ the rotational relaxation effects cancel out and the fluorescence yield is close to that with no RET consideration. Studying the temperature effect, we observe the fluorescence quantum yield from low temperature to high temperature decreases nearly 40%, much more than the 20% expected from quenching considerations alone, and only highly predissociative levels are relatively insensitive to collisional rate changes. Using rotational levels below B $v' = 1$ $N' = 8$, the quantum yield will be more sensitive to collisions than in B $v' = 0$. The least complex choices for flame diagnostics in B $v' = 1$ are $N = 8$, 9, or 10, but only $N' = 8$ offers enough signal in the present experimental conditions.

5.2 Vibrational and electronic energy transfer

The analysis of vibrational and electronic energy transfer compared to total collisional removal from B $v' = 0$ (Q_B) is given by the expression:

$$\frac{ET(\mathrm{B} \rightarrow \mathrm{F})}{Q_B} = \frac{I_F}{I_B}\frac{A_{Bi}}{A_{Fi}}\frac{\left(Q_F + \sum A_{Fi}\right)}{Q_B} \qquad (4)$$

where ET is the collisional transfer rate between B and F states, F is the final state (either B $v' = 0$ or A state), I_i is the fluorescence intensity, Q_i is the appropriate quenching rate (in the A state case, the quenching is weighted by the vibrational populations), and A_i is the emission coefficient for the observed vibrational band. Applying this expression, we find 24% VET transfer within the $B\,^2\Sigma^-$ state ($v' = 1 \rightarrow v' = 0$). There is 30% electronic energy transfer (EET) B $v' = 1 \rightarrow A\,^2\Delta$ transfer. No significant rotational dependence of these processes is seen (Table 4). Although, reverse process contributions are negligible to the measured collisional transfer rates, the vibrational energy transfer to B $v' = 0$ is large enough and we have to remove the EET contribution from B $v' = 0$ to A. Using the experimental data of Garland and Crosley [23], the EET B $v' = 1 \rightarrow$ A transfer is 24% of the total collisional removal in the B $v' = 0$ manifold. The rotational distributions of collisionally populated vibrational levels appear thermalized at ≈ 2000 K, as was observed in the analogous experiment [23]. Note that the transfer is independent of predissociation in the initial state; thus, for a rotationally independent energy transfer rate, we find the fluorescence intensity ratios $B(v = 0)/B(v = 1)$ and $A/B(v = 1)$ the same regardless of the predissociation rate in the initial $B\,^2\Sigma^-$ $v' = 1$ state (see Fig. 5).

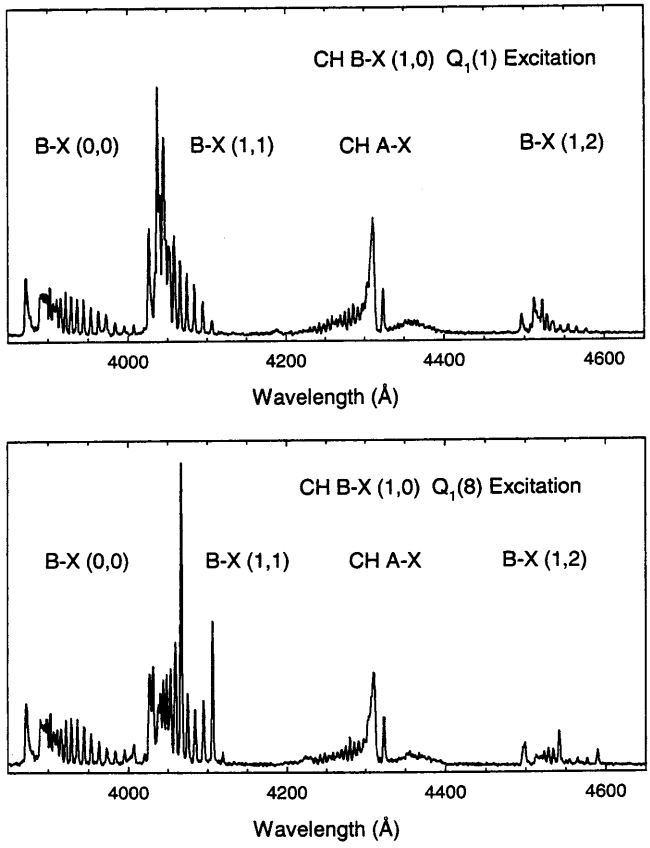

Fig. 5. CH B−X and A−X dispersed fluorescence spectra after pumping CH B−X (1,0) $Q_1(1)$ and $Q_1(8)$ in the methane/air flame at atmospheric pressure resolved with 0.25 nm resolution and total time-integrated fluorescence

The vibrational energy transfer $B\,^2\Sigma^-\, v' = 1 \rightarrow v' = 0$ ratio VET/Q was estimated to be 8.5% by Garland and Crosley [23] after applying the detailed balance principle to the $B\,v' = 0 \rightarrow v' = 1$ transfer rate value. Reanalysis of these data using new transition probabilities of Luque and Crosley [17] brings the value to 12%. Moreover, evaluating the amount of population from $B\,v' = 0$ transferred to the predissociative levels in $v' = 1$, which is nearly 50% at 1900 K; we find that the correct ratio of VET/Q $B\,v' = 1 \rightarrow v' = 0$ must be around 25%, three times larger than initially estimated, and in very good agreement with the present experiment.

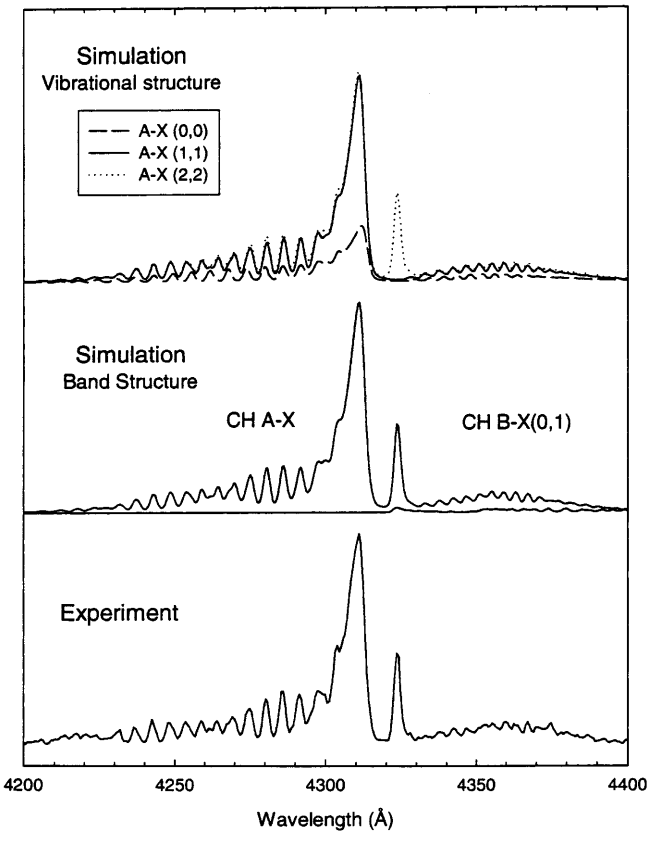

Fig. 6. Dispersed fluorescence spectra of CH A−X after pumping CH B−X (1,0) $Q_1(7)$ taken with 0.25 nm FWHM resolution (*lower panel*). Simulated spectra showing the A−X and B−X (0,1) contributions (*center panel*). Contributions from the A state vibrational levels with population ratios $N(0) : N(1) : N(2)$ 0.22 : 0.48 : 0.27. Rotational temperatures are 2000 K (*upper panel*)

Garland and Crosley [23] measured (22 ± 6)% EET/Q for the $B\,(v' = 0) \rightarrow A\,^2\Delta$ process, the same as the (24 ± 3)% measured from $B\,v' = 1$. Those values point out no dependence of EET with vibrational level. We use spectral simulation (Fig. 6) to study the vibrational branching ratios. LIFBASE [33] includes the emission coefficients and predissociation rates. Quenching rates are taken as 0.35, 0.4, and 0.6 $\mu s^{-1}Torr^{-1}$ for $A\,v' = 0, 1, 2$, according to the observations by Tamura et al. [38] and Luque and coworkers [25, 42]. The vibrational populations obtained from simulation need minor corrections by VET in the A state, and by the contribution of EET from $B\,v' = 0$. The vibrational transfer (VET/Q) in the A state has been found ≤ 10% in flame conditions [23], so we use the upper value to correct our populations. The EET from $B\,v' = 0$ is 20% of the total collisional removal, and the branching ratios, 80% $A\,v' = 1$ and 20% $v' = 0$ [23] are used to retrieve the actual populations. The nascent vibrational distribution in A state after EET turned out to be inverted with averaged ratios $N(0) : N(1) : N(2) : N(3)$ of 0.17 : 0.49 : 0.31 : (< 0.03). A simple exponential gap law for EET can describe the vibrational population ratios.

$$R(E_i \rightarrow E_f) = g_f e^{\left(\frac{(E_i - E_>)}{kT}\right)} b \times e^{\left(\frac{-\beta|E_f - E_i|}{kT}\right)} \qquad (5)$$

β is found to be ≈ 0.6, $b \approx 2 \times 10^7\ s^{-1}$, E_i is the energy of the vibrational level i at $N' = 0$, g_f is the electronic degeneracy of the final state. A vibrational overlap integral model, substituting the second exponential term by the overlap integral between the two vibrational levels involved can also be constructed. Table 5 shows the calculated relative rate constants using the two models for transfer from $B\,v' = 0$ and 1. Vibrational overlap model predictions between $B\,v' = 1$ and $A\,v' = 0 - 3$ correlate with the energy gap model predictions, but there is not enough evidence to support this mechanism for the observed electronic energy transfer. Garland and Crosley [23] found that the distribution in A state after transfer from $B\,v' = 0$ is mostly $A\,v' = 1$ (> 80%), in disagreement with a simple prediction from favorable overlap integrals in the transfer mechanism.

There does appear to be a moderate branching-ratio dependence on the initially excited rotational number in $B\,v' = 1$ in the present experiments. The percentage of transfer into $v' = 0$ decreases with N number; $v' = 2$ shows the

Table 5. Calculations for the branching ratios into the A state populated by electronic energy transfer (EET) using an energy gap ($E_B - E_A$) and overlap integral ($q_{v'v''}$) based models

B(1) → A(v)	$q_{v'v''}$	$E_B - E_{A(v)}$ (cm^{-1})	Energy gap model ($\beta = 0.6$)	Overlap integral model	Experiment
1 → 0	0.16	4275	0.15	0.24	0.17 ± 0.03
1 → 1	0.34	1538	0.52	0.51	0.49 ± 0.03
1 → 2	0.34	−1006	0.31	0.22	0.31 ± 0.04
1 → 3	0.12	−3331	0.02	0.02	< 0.03
B(0) → A(v)	$q_{v'v''}$	$E_B - E_A(v)$ (cm^{-1})	Energy gap model ($\beta = 0.6$)	Overlap integral model	Experiment [23]
0 → 0	0.79	2480	0.30	0.850	≤ 0.2
0 → 1	0.18	−257	0.67	0.148	> 0.8
0 → 2	0.02	−2801	0.03	0.002	

opposite trend (Table 4). This behavior can be understood from the energy gap standpoint, because increasing the rotational number of the level pumped in B $v' = 1$ brings the initial population energetically closer to A $v' = 2$ and further away from A $v' = 0$. Modeling the initial rotational level dependence is not straightforward since the rotational relaxation in B $v' = 1$ washes out the energy gap effect partially. Qualitatively correct branching-ratio predictions can be obtained when the populations from the rotational relaxation model are used to calculate the effective rotational energy for the energy gap model. If we apply this principle to the transfer from B $v' = 0$, the percentage transferred to A $v' = 1$ will increase with rotational level excited in B $v' = 0$, bringing experimental observations and model calculations to better agreement.

We investigated the energy-transfer dependence on temperature and flame composition by dividing the CH profile in two regions with temperatures from $\approx$ 1100 to 1700 K and 1700 to 2000 K. We did not find differences in the ratios B $(v' = 0)$/B $(v' = 1)$ and A/B $(v' = 1)$ in the two regions, although the noise in the lower temperature region, where there is little CH, makes this estimation to have an uncertainty of 15%. The constant energy-transfer ratios suggests that Q, VET, and EET have similar dependencies with temperature and composition in both CH A and B. This is an important practical consequence for LIF applications: from (4) we find that I_F is directly proportional to I_B, independent of the flame conditions, and this validates energy transfer schemes for PLIF on CH B $v' = 1$, as has been shown for CH B $v' = 0$ [24]. These schemes must also be corrected by fluorescence quantum yield variations in the B $v' = 1$ state in order to obtain fully quantitative results. Another positive consequence is that the additional fluorescence after exciting the CH B $v' = 1$ levels can be used to increase the LIF signal levels without losing accuracy in the measured CH spatial distribution. The amount of light from the VET and EET produced B$-$X (0,0) and A$-$X $(v', v'' = v)$ bands accounts for $\approx$ 26% and 27%, respectively, of the total fluorescence between 380 and 450 nm in the present flame; thus, the fluorescence signal can be increased a factor of two compared to the detection of the B$-$X (1,1) band only.

6 Conclusions and implications for flame diagnostics

We have studied collisional transfer processes in CH B $v' = 1$, exciting both non-predissociative and predissociative levels in methane flames. The fluorescence yields for all the levels are modified by the combination of rotational relaxation and rotationally dependent predissociation. Simple RET models are sufficient to test the reliability of predissociative LIF schemes, and the parameters are relatively independent of flame composition. Vibrational and electronic energy transfer are competitive. Light from levels populated by vibrational and electronic transfer account for a large part of the total fluorescence, and are constant irrespective of the predissociation degree of the initially excited CH B $v' = 1$ level. Predissociative laser-induced fluorescence schemes using CH B $v' = 1$ are not as effective as expected for reduction of collisional dependence. The most promising candidate for excitation at atmospheric pressure is $N' = 8$ ($\tau \approx 0.35$ ns), which shows at flame temperatures fluorescence quantum yield variations comparable to non-predissociative levels in CH B $v' = 0$. The CH B $v' = 1$, $N' = 9$ and 10 levels are more resilient to collisions but their signal levels are low for typical flame diagnostics and experiments exciting these levels are expected to be more difficult. Moreover, the high laser fluences needed to pump the highly predissociative levels $N' = 9$ and 10 are likely to produce problems to interpret the fluorescence because of the ground state rotational energy transfer effects in the dynamics of the optical pumping as pointed out by Rothe et al. [29]. In spite of exciting a predissociative level, an estimate of the signal level exciting B $v' = 1$, $N' = 8$ and detecting B$-$X (1,1) compared to exciting B $v' = 0$, $N' = 8$ and detecting B$-$X (0,1) and CH A$-$X produced by energy transfer from B $v' = 0$, reveals that the fluorescence signal from both schemes is going to be very similar for equivalent optical pumping rates.

The $(1, 0)/(1, 1)$ excitation/detection CH LIF schemes are effective to remove Rayleigh and Mie scattering, although some Raman signals can appear along with the LIF. These schemes are less likely to suffer from sample self-absorption, since most emission is a resonant transition to sparsely populated levels in the ground state. Also, the laser absorption through the sample is less, because the absorption coefficients for the (1,0) bands are smaller than those of the (0,0) bands in the CH electronic systems. The fluorescence collection factors are large, because the emission is detected in strong diagonal bands. Finally, the population percentage of molecules available to be excited is at the maximum attainable at flame temperatures, because the excitation is from the lowest vibrational level $v'' = 0$, the one always most populated at flame conditions.

Comparison of the $(1, 0)/(1, 1)$ schemes using A$-$X, B$-$X, C$-$X at atmospheric pressure shows the following. The C$-$X (1,0) excitation seems to have a good prognosis attending to overall oscillator strengths and fluorescence quantum yield collisional variations, although the predissociation rates and collisional behavior of CH C $v' = 1$ are not well known. A$-$X has the problem of small oscillator strength for off-diagonal bands, and the fluorescence yield variation should be just 20% in the range 1200–2000 K. Finally, the B$-$X system fluorescence yield variation is comparable to A$-$X when the levels pumped are $N' = 8$ or 9, but the oscillator strength is one hundred times larger, which may be important if laser power availability is a factor and laser absorption through the sample is not an issue.

Acknowledgements. This work was funded by the Basic Research Group of the Gas Research Institute.

References

1. R.H. Barnes, C.E. Moeller, J.F. Kircher, C.M. Berber: Appl. Opt. **12**, 2531 (1973)
2. M.J. Dyer, D.R. Crosley: In Proceeding of the International Conference on Lasers '84 (1984) p. 211
3. P. Andresen, A. Bath, W. Groger, H.W. Lulf, G. Meijer, J.J. ter Meulen: Appl. Opt. **27**, 365 (1988)
4. P. Andresen, G. Meijer, H. Schluter, H. Voges, A. Koch, W. Hentschel, W. Oppermann, E. Rothe: Appl. Opt. **29**, 2392 (1990)
5. M.G. Allen, R.D. Howe, R.K. Hanson: Opt. Lett. **11**, 126 (1985)
6. R. Bombach, B. Kappeli: Appl. Phys. B **68**, 251 (1999)
7. K.T. Walsh, M.B. Long, M.A. Tanoff, M.D. Smooke: In Twenty-Seventh Symposium (International) on Combustion (The Combustion Institute, Boulder, CO 1998) p. 615
8. Y.C. Chen, M.S. Mansour: Appl. Phys. B **64**, 599 (1997)

9. P.M. Doherty, D.R. Crosley: Appl. Opt. **23**, 713 (1984)
10. P.H. Paul, J.E. Dec: Opt. Lett. **19**, 998 (1994)
11. J. Luque, D.R. Crosley: J. Chem. Phys. **104**, 2146 (1996)
12. M. Namazian, R.L. Schmitt, M.B. Long: Appl. Opt. **27**, 3597 (1988)
13. V. Bergemann, W. Meier, D. Wolff, W. Stricker: Appl. Phys. B **66**, 489 (1998)
14. A. Hirano, M. Ippommatsu, M. Tsujishita: Opt. Lett. **17**, 303 (1992)
15. M. Tsujishita, M. Ipponmatsu, A. Hirano: Jpn. J. Appl. Phys. **32**, 5564 (1993)
16. J.B. Jeffries, R. Copeland, D.R. Crosley, J. Quant. Spectrosc. Radiat. Transfer **37**, 419 (1987)
17. J. Luque, D.R. Crosley: J. Chem. Phys. **1996**, 3907 (1996)
18. W. Ubachs, G. Meyer, J.J. ter Meulen, A. Dymanus: J. Chem. Phys. **84**, 3032 (1986)
19. J. Brzozowski, P. Bunker, N. Elander, P. Erman: Astrophys. J. **207**, 414 (1976)
20. J.B. Jeffries, R.A. Copeland, G.P. Smith, D.R. Crosley: In Twenty-first Symposium (International) on Combustion (The Combustion Institute 1986) p. 1709
21. C.D. Carter, J.M. Donbar, J.F. Driscoll: Appl. Phys. B **66**, 129 (1998)
22. R.J.H. Klein-Douwel, J.J.L. Spaanjaars, J.J. ter Meulen: J. Appl. Phys. **78**, 2086 (1995)
23. N.L. Garland, D.R. Crosley: Appl. Opt. **24**, 4229 (1985)
24. K.J. Rensberger, R.A. Copeland, M.L. Wise, D.R. Crosley: In Twenty-second Symposium (International) on Combustion (The Combustion Institute 1988) p. 1867
25. J. Luque, D.R. Crosley: Appl. Opt. **99**, 1423 (1999)
26. J. Luque, D.R. Crosley: Chem. Phys. **206**, 185 (1996)
27. P. Beaud, P.P. Radi, D. Franzke, H.M. Frey, B. Mischler, A.P. Tzannis, T. Gerber: Appl. Opt **37**, 3354 (1998)
28. T. Nielsen, F. Bormann, M. Burrows, P. Andresen: Appl. Opt. **30**, 7960 (1997)
29. E.W. Rothe, Y.W. Gu, G.P. Reck: Appl. Opt. **35**, 934 (1996)
30. T.A. Brunner, N. Smith, A.W. Karp, D.E. Pritchard: J. Chem. Phys. **74**, 3324 (1981)
31. R. Fei, H.M. Lambert, T. Carrington, S.V. Filseth, C.M. Sadowski, C.H. Dugan: J. Chem. Phys. **100**, 1190 (1190)
32. G. Herzberg, J.W.C. Jones: Ap. J. **158**, 399 (1969)
33. J. Luque, D.R. Crosley: LIFBASE version 1.61 edn. (SRI International, MP-99-0099 (www.sri.com/cem/lifbase) 1999)
34. N. Elander, M. Hehenberger, P.R. Bunker: Phys. Scripta **20**, 631 (1979)
35. A. Kumar, C.C. Hsiao, W.C. Hung, Y.P. Lee: J. Chem. Phys. **109**, 3824 (1998)
36. P.G. Szalay, L. Nemes: Mol. Phys. **96**, 359 (1999)
37. N. Heberle, G.P. Smith, J.B. Jeffries, D.R. Crosley, R.W. Dibble: Combust. Flame, to be published (2000)
38. M. Tamura, P.A. Berg, J.E. Harrington, J. Luque, J.B. Jeffries, G.P. Smith, D.R. Crosley: Combust. Flame **114**, 502 (1998)
39. R.G. Joklik, J.W. Daily: Combust. Flame **69**, 211 (1987)
40. W. Qingyu, M. Yang, Y. Li: J. Electrochem. Soc. **137**, 3099 (1990)
41. K.L. Steffens, J. Luque, J.B. Jeffries, D.R. Crosley: J. Chem. Phys. **106**, 6262 (1997)
42. J. Luque, J. Ruiz, M. Martin: Laser Chem. **14**, 207 (1994)
43. N.H. Brooks, W.H. Smith: Astrophys. J. **194**, 513 (1974)
44. C.C. Wang, L. Nemes, K.C. Lin: Chem. Phys. Lett. **245**, 585 (1995)